Effect of Plan Configuration on Seismic Performance of Single-Story Wood-Frame Dwellings

Kraisorn Lucksiri[1]; Thomas H. Miller, M.ASCE[2]; Rakesh Gupta, M.ASCE[3]; Shiling Pei, M.ASCE[4]; and John W. van de Lindt, M.ASCE[5]

Abstract: A numerical investigation is presented on effects of plan configuration on seismic responses of single-story, wood-frame dwellings. 151 models were developed using observations of 412 dwellings of rectangular, L, T, U, and Z-shapes in Oregon. A nonlinear, time-history program, Seismic Analysis Package for Wood-frame Structures, was the analysis platform. Models were analyzed for 10 pairs of biaxial ground motions (spectral accelerations from 0.1 g to 2.0 g) for Seattle. Configuration comparisons were made using median shear wall maximum drifts and occurrences of maximum drifts exceeding the 3% collapse prevention limit. Plan configuration significantly affects performance through building mass, lateral stiffnesses, and eccentricities. Irregular configuration tends to induce eccentricity and cause one wall to exceed the allowable drift limit, and fail, earlier than others. Square-like buildings usually perform better than long, thin rectangles. Classification of single-story dwellings based on shape parameters, including size and overall aspect ratio, plan shape, and percent cutoff area, can organize a building population into groups having similar performance and be a basis for including plan configuration in rapid visual screening. **DOI: 10.1061/(ASCE)NH.1527-6996.0000061.**

CE Database subject headings: Seismic analysis; Wood structures; Configuration; Residential buildings.

Author keywords: Seismic analysis; Wood structures; Configuration.

Introduction

Wood-frame construction is the most common structural type for houses in North America. It is relatively light weight, flexible, and inherently redundant in its force resisting systems, all beneficial properties for buildings subjected to earthquakes. However, the Northridge earthquake (Schierle 2003) has shown that small wood-frame dwellings are seismically vulnerable to earthquake damage at different levels from minor nonstructural damage, i.e., gypsum wall board (GWB) cracking to an uninhabitable level. Approximately, $20 billion of the $40 billion in losses caused by the Northridge earthquake were the result of wood-frame building damage, virtually all residential.

Vulnerability assessment of wood-frame dwellings can be initiated by performing a rapid visual screening (RVS) to obtain preliminary information on whether an engineering evaluation and/or structural rehabilitation are needed. Examples of currently available RVS tools are the second edition of FEMA 154 (FEMA 2002a), its supporting document FEMA 155 (FEMA 2002b), and ATC 50 (ATC 2007). In ATC 50, some features such as foundation connections, cripple walls, and unreinforced chimneys are relatively easy to identify and it is easy to decide to rehabilitate as they are obviously potential sources of damage. This is, however, not the case for features like plan configuration (shape, including aspect ratio) and irregularity, where the effect varies from case to case and depends on the type (reentrant corner, door/window opening, etc.) and degree of irregularity (size of door/window opening, offset ratio of reentrant corner, etc.). This limitation, found in both FEMA 154 and ATC 50, has become the motivation for this study.

Inclusion of plan configuration and irregularity in an RVS procedure is a challenging task, as wood-frame houses vary widely in layout. A numerical model is needed to capture the complexity of building plan irregularities and to provide realistic predictions for a large number of analyses. Plan irregularity is approximately addressed in FEMA 154 by simply increasing the input spectral acceleration response values by 50%. Here, the Seismic Analysis Package for Wood-frame Structures (SAPWood) (Pei 2007; Pei and van de Lindt 2007) is used to directly handle effects of plan configuration and irregularity.

This study initiates an approach to include plan configuration and irregularity in RVS. The objectives are (1) to propose a way to classify single-story, wood-frame dwellings into groups based on a set of shape parameters and (2) to numerically investigate the effect of plan irregularity, resulting from plan configuration, on seismic performance. Other sources of plan irregularities such as unbalanced stiffnesses caused by large openings (windows and garage doors) are not included at this stage but will be a part of the next study. Models for case study are all single-story buildings. The state of Oregon is the focus area for the study. Comparisons of performance are based on maximum shear wall drifts.

[1]Graduate Student, School of Civil and Construction Engineering and Dept. of Wood Science and Engineering, Oregon State Univ., Corvallis, OR 97331. E-mail: kraisorn.lucksiri@oregonstate.edu

[2]Associate Professor, School of Civil and Construction Engineering, Oregon State Univ., Corvallis, OR 97331 (corresponding author). E-mail: thomas.miller@oregonstate.edu

[3]Professor, Dept. of Wood Science and Engineering, Oregon State Univ., Corvallis, OR 97331. E-mail: rakesh.gupta@oregonstate.edu

[4]Assistant Professor, Dept. of Civil and Environmental Engineering, South Dakota State Univ., Brookings, SD 57006. E-mail: Shiling.Pei@sdstate.edu

[5]Professor and Drummond Chair, Dept. of Civil, Construction, and Environmental Engineering, Univ. of Alabama, Tuscaloosa, AL 35487. E-mail: jwvandelindt@eng.ua.edu

Note. This manuscript was submitted on July 19, 2010; approved on June 6, 2011; published online on June 8, 2011. Discussion period open until July 1, 2012; separate discussions must be submitted for individual papers. This paper is part of the ***Natural Hazards Review***, Vol. 13, No. 1, February 1, 2012. ©ASCE, ISSN 1527-6988/2012/1-24–33/$25.00.

Plan Configuration Observation

There are numerous plan configurations possible for residential buildings but not all of them are commonly used in design. Therefore, the first step was to determine commonly used plan configurations (shapes) for single-story existing dwellings. Although reviewing construction drawings or an on-site survey of buildings would provide more accurate data, a different approach was used to save time and cost for the large number of houses throughout the state. Thus, Google Earth and Google SketchUp were used. Google Earth displays satellite images of the earth's surface whereas Google SketchUp is a 3D modeling program capable of working together with Google Earth.

The observation process was a two-step task: city selection and pin point (specific coordinates within a selected city) selection. City selection was based on 241 Oregon cities and their population obtained from the Census Bureau's Population Estimates Program (U.S. Census Bureau 2009), vintage 2007. Based on their estimate, there are 168 cities (70%) that have population less than 5,000 but only 26 cities (11%) having population over 20,000. To ensure that samples were collected from different size cities, this study organized cities into: group A ($0 <$ population $\leq 5{,}000$), group B ($5000 <$ population $\leq 20{,}000$), and group C (population $> 20{,}000$). Ten cities were then randomly selected from each group as shown in Table 1. Five simple geometries commonly used for wood-frame dwellings were selected for the study, including rectangle, L, T, U, and Z-shapes.

Before selection of pin points could be made from within a city, boundaries of the city were established with two pairs of latitude and longitude lines embracing most of the buildings in the city. This excluded lakes, forest, or agricultural lands with few residential buildings. Pin points, located within that city boundary, were then randomly generated in terms of latitude-longitude pairs. Guidelines for pin points and sample selection were:

1. Each pin point represents the center of an observational area.
2. Houses that have shapes of interest, located within a 76.2 m (250 ft) radius from the pin point, and within a residential area, are sample candidates.
3. Plan area of a sample house did not exceed 464 m^2 (5,000 ft^2).
4. A reentrant corner is considered to exist if it is at least 1.22×1.22 m (4×4 ft).
5. As many dwellings were assessed as possible for each pin point. However, dwellings with exactly the same configuration were assessed only once.
6. Twenty pin points was the overall limit for each city.

The number of samples (for each plan shape) from each group was determined based on the relative population among groups (A:B:C) which is approximately 1:2:7 (Table 2). With a limit of 20 pin points per city, total numbers of actual observed samples were 95, 100, 84, 61, and 72 for rectangular, L, T, U, and Z-shapes, respectively. Fig. 1 shows the details and notation for the observed parameters for five shapes of interest (rectangle, L, T, U, and Z-shapes). Table 3 shows a summary of observed parameters for these actual houses. These were used to determine the range of parameters for model houses as shown in Table 3 as well.

Case Study Configurations

Dimensions of all observed buildings were transformed into two groups of parameters as shown in Fig. 1. The first group of key parameters are those used in the case study matrix including (1) overall shape ratio, R, (2) percent cutoff, C_p, (3) cutoff shape ratio, R_c, and (4) cutoff ratio, C_r (for T, U, and Z-shapes). The R and C_p parameters are related to overall floor proportions and the reduction in area cut off from the base rectangle ($a \times b$) that encloses the entire plan area. R_c reflects the shapes of the cutoff areas whereas C_r indicates distribution of cutoff areas in a floor plan. For a given set of R and C_p values, variation of R_c and C_r yields different plan shapes, locations of exterior shear walls and, consequently, eccentricities between the center of rigidity and center of mass of buildings. This is based on the assumption that unit shear strength is the same for all wall lines. Different nail spacings for wall lines with large openings should also be investigated. The second group of supporting parameters defines the geometries of reentrant corners. Key parameters varied within the most extreme values, with limits constrained by the supporting parameters. A summary of all parameters is shown in Fig. 1, with values in Table 3.

This study classifies buildings into 3 configuration levels: index level, subindex level, and sub-sub-index level. The index level classifies buildings by their shapes: rectangles, L, T, U, and Z-shapes, with overall box area ($a \times b$) of 139 sq m (1,500 sq ft). The subindex level includes index level buildings with a specific set of R and C_p values. Three selected values of R and C_p, determined based on the observed mean $\pm 2^*$ standard deviation (SD) range and the corresponding maximum and minimum values, for each index level building are shown in the Selected range column in Table 3. For example, for L-shape index buildings, the selected values are: $R = 0.5$, 0.75, 1.00, and $C_p = 10\%$, 20%, and 30%; thus, nine L-shape subindex groups with different combinations of R and C_p, can be developed. Finally, each of the subindex level buildings

Table 1. Randomly Selected Cities in Each Group

Group A			Group B			Group C		
No.	City	Population[a]	No.	City	Population[a]	No.	City	Population[a]
A-1	Nyssa	3,026	B-1	Canby	15,602	C-1	Corvallis	51,125
A-2	Shady Cove	2,299	B-2	Molalla	7,115	C-2	Redmond	23,769
A-3	Gervais	2,416	B-3	Sutherlin	7,201	C-3	Beaverton	90,704
A-4	Coburg	1,021	B-4	Wilsonville	18,814	C-4	Albany	47,239
A-5	Yoncalla	1,047	B-5	Talent	6,150	C-5	Keizer	35,312
A-6	North Plains	1,813	B-6	Central Point	16,447	C-6	Medford	72,186
A-7	Heppner	1,371	B-7	Lebanon	14,836	C-7	Springfield	56,666
A-8	Brownsville	1,620	B-8	North Bend	9,672	C-8	Woodburn	22,044
A-9	Siletz	1,098	B-9	Happy Valley	11,599	C-9	Newberg	22,193
A-10	Joseph	959	B-10	Troutdale	15,366	C-10	Salem	151,913

[a]Source: U.S. Census Bureau 2009.

Nat. Hazards Rev., 2012, 13(1): 24-33

Table 2. Determination of Population Weights among City Groups

	Group			
	A	B	C	Total[a]
Population	0–5,000	5,001–20,000	> 20,000	
No. of cities	168	47	26	241
Total population	219,894	492,927	1,854,266	2,567,087
Relative population	8.6%	19.2%	72.2%	100.0%
Sample weight	1	2	7	10

[a]Source: U.S. Census Bureau 2009.

was assigned R_c and C_r, based on the selected ranges shown in Table 3, to yield the final building shapes as follows:

- L-shape: Three different values of R_c were assigned to each subindex to represent the minimum and maximum cutoff shape ratios and a square cutoff.
- T-shape: For each subindex, offset distances, f and d, were assumed equal. Two cutoff ratios (1.0 and minimum) representing equal and unequal cutoffs were included.
  - Equal cutoffs ($C_r = 1.0$): Three values of R_{c1} were assigned to each subindex for minimum and maximum cutoff shape ratios and square cutoffs. Since the offset distance f was assumed to equal d, $Rc_1 = Rc_2$.
  - Unequal cutoffs (minimum C_r): Each of the sub-subindex buildings developed previously for equal cutoffs was used as a basis for the unequal cutoffs' case. With the distance f (and d) kept constant, the distances c and e were varied to achieve the smallest C_r that kept the supporting parameters within their ranges. For example, buildings T1 and T4 are a pair, and their f and d distances are equal. The c and e distances are equal for building T1 but not T4.
- U-shape: Equal leg lengths ($e = g$) were assumed, i.e., the cutoff ratio (C_r) is zero, and there are equal widths ($R_l = 1.0$). Three values of R_c were assigned to each subindex building to represent the minimum and maximum cutoff shape ratios and a square cutoff.
- Z-shape: Two cutoff ratios ($C_r = 1.0$ and minimum C_r) representing equal cutoffs and unequal cutoffs were included. For each C_r, five combinations of cutoff shape ratios were used including: (1) [min. R_{c1}, min. R_{c2}], (2) [min. R_{c1}, max. R_{c2}], (3) [max. R_{c1}, min. R_{c2}], (4) [max. R_{c1}, max. R_{c2}], and (5) [$R_{c1} = 1.0$, $R_{c2} = 1.0$]. The values of C_r, R_{c1}, and R_{c2} are determined so the related supporting parameters are still within their ranges.

Cases where the values of either R_c or C_r do not keep all supporting parameters in their ranges were excluded. As a result, 151 sample models (Fig. 2) are developed: 4 rectangles, 21 L-shapes, 35 T-shapes, 18 U-shapes, and 73 Z-shapes.

Structural Modeling

Buildings were modeled to represent typical wood-frame, single-story dwellings in North America. Vertical elements consist of interior gypsum wallboard (GWB) partition walls and exterior structural shear walls, all assumed to be 2.44 m (8 ft) in height. 50% of each side of the building perimeter was assumed to consist of shear walls, contributing to the lateral force resisting system. This 50% shear walls assumption was selected to conservatively satisfy the residential codes adopted by the state of Oregon over different periods of time, such as CABO (1989, 1995) and the International Residential Code (ICC 2000). The requirements from CABO (1989, 1995) and ICC (2000) (for seismic design category A, B, and C) are to provide a minimum of 1.22 m (48 in) structural

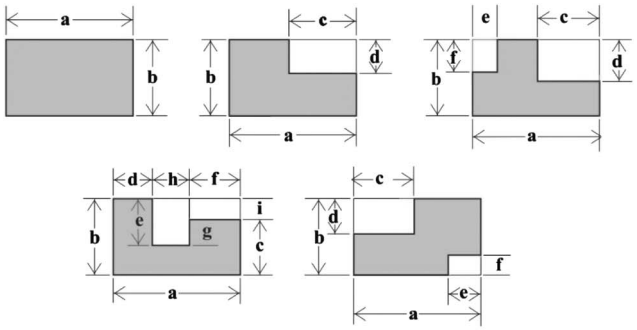

Plan Shape	Properties
Rectangle	Key parameters: Overall shape ratio: $R = \frac{b}{a}$ Supporting parameters: N/A
L-Shape	Key parameters: Overall shape ratio: $R = \frac{b}{a}$ Percent cutoff: $C_p = \left(\frac{c*d}{a*b}\right) * 100$ Cutoff shape ratio: $R_c = \frac{d}{c}$ Supporting parameters: c/a, d/b
T-Shape	Key parameters: Overall shape ratio: $R = \frac{b}{a}$ Percent cutoff: $C_p = \left(\frac{(c*d)+(e*f)}{a*b}\right) * 100$ Cutoff shape ratio: $R_{c1} = \frac{d}{c}$ Cutoff shape ratio: $R_{c2} = \frac{f}{e}$ Cutoff ratio: $C_r = \frac{(e*f)}{(c*d)}$ Supporting parameters: e/c, d/f, c/a, e/a, d/b, f/b
U-Shape	Key parameters: Overall shape ratio: $R = \frac{b}{a}$ Percent cutoff: $C_p = \left(\frac{(h*e)+(f*i)}{a*b}\right) * 100$ Cutoff shape ratio: $R_c = \frac{h}{e}$ Width ratio of legs: $R_l = \frac{f}{d}$ Cutoff ratio: $C_r = \frac{(f*i)}{(h*e)}$ Supporting parameters: c/b, e/b, h/a
Z-Shape	Key parameters: Overall shape ratio: $R = \frac{b}{a}$ Percent cutoff: $C_p = \left(\frac{(c*d)+(e*f)}{a*b}\right) * 100$ Cutoff shape ratio: $R_{c1} = \frac{d}{c}$ Cutoff shape ratio: $R_{c2} = \frac{f}{e}$ Cutoff ratio: $C_r = \frac{(e*f)}{(c*d)}$ Supporting parameters: c/a, e/a, d/b, f/b, e/c, f/d

Fig. 1. Plan shape properties and notation; for T- and Z-shapes, $(c*d) > (e*f)$

sheathing wall located at each end and at least every 25 feet of wall length, but not less than 16% of braced wall line. For buildings with seismic design category D_1 or D_2 (ICC 2000), a similar requirement is applied but with the minimum wall lengths of 20% and 25% of braced wall line, respectively.

A pilot study was also performed regarding percent openings in existing buildings. Focusing on rectangular, L, T, U, and Z plan shapes, observations were made of 98 single-story dwellings in

Table 3. Summary of Observed Parameters and Selected Ranges for Modeling

Shapes	Parameters	Observed ranges	Mean ± 2SD	Selected ranges
Rect. $N = 95$	R	0.29 to 1.00	0.36 to 0.98	0.35, 0.50, 0.75, 1.00
L-Shape $N = 100$	R	0.48 to 1.00	0.57 to 1.08	0.50, 0.75, 1.00
	C_p	3% to 31%	3% to 34%	10%, 20%, 30%
	R_c	0.13 to 3.00	−0.19 to 1.68	0.20, 1.00, 1.60
	c/a	0.12 to 0.70	0.20 to 0.70	0.20 to 0.70
	d/b	0.11 to 0.63	0.12 to 0.59	0.20 to 0.60
T-Shape $N = 84$	R	0.43 to 1.47	0.44 to 1.27	0.50, 1.00, 1.30
	C_p	8% to 38%	6% to 33%	10%, 20%, 30%
	C_r	0.14 to 1.00	0.07 to 1.16	0.20, 1.00
	R_{c1}	0.21 to 6.00	−0.75 to 3.62	0.30, 1.00, 3.60
	R_{c2}	0.23 to 11.25	−0.96 to 5.74	0.30, 1.00, 5.80
	e/c	0.14 to 2.00	0.01 to 1.29	0.20 to 1.30
	d/f	0.60 to 2.12	0.6 to 1.52	1.00
	c/a	0.13 to 0.61	0.12 to 0.49	0.10 to 0.50
	e/a	0.07 to 0.36	0.04 to 0.33	
	d/b	0.15 to 0.71	0.14 to 0.70	0.20 to 0.70
	f/b	0.13 to 0.73	0.12 to 0.69	
U-Shape $N = 61$	R	0.36 to 1.35	0.44 to 1.27	0.5, 1.0, 1.3
	C_p	3% to 27%	1% to 20%	5%, 10%, 15%
	C_r	0 to 4.67	−0.87 to 2.66	0
	R_l	0.47 to 1.38	0.52 to 1.25	1.00
	R_c	0.17 to 3.25	−0.59 to 2.29	0.20, 1.00, 2.30
	c/b	0.62 to 1.00	0.67 to 1.09	1.0
	e/b	0.14 to 0.62	0.14 to 0.52	0.20 to 0.60
	h/a	0.06 to 0.48	0.03 to 0.34	0.10 to 0.40
Z-Shape $N = 72$	R	0.54 to 1.00	0.59 to 1.01	0.50, 0.75, 1.00
	Cp	9% to 39%	10% to 34%	10%, 20%, 30%
	R_{c1}	0.14 to 3.50	−0.24 to 2.21	0.20, 1.00, 2.20
	R_{c2}	0.14 to 6.00	−1.05 to 4.81	0.20, 1.00, 4.80
	C_r	0.20 to 1.00	0.13 to 1.03	0.30, 1.00
	c/a	0.15 to 0.71	0.13 to 0.63	0.20 to 0.70
	e/a	0.07 to 0.65	−0.05 to 0.55	0.10 to 0.60
	d/b	0.12 to 0.70	0.15 to 0.64	0.20 to 0.60
	f/b	0.08 to 0.65	0.09 to 0.67	0.10 to 0.60
	e/c	0.17 to 2.00	−0.086 to 1.46	0.20 to 1.50
	f/d	0.25 to 2.01	0.29 to 1.68	0.30 to 1.60

Corvallis, Oregon. It was found that the average percent openings (resulting from doors and windows) along the long and short sides are 50% (S.D. = 11%) and 20% (S.D. = 17%), respectively. The overall ranges are 20–75% on the long side and 0–60% on the short side. Since most houses in Oregon have structural sheathing around the entire perimeter with the same nailing schedule, the 50% assumption is thus considered a reasonable and conservative value for this comparative study of plan shapes. The seismic performance of existing houses designed with different amounts of openings will obviously vary, i.e., the more openings, the less the stiffness and the greater the lateral drift. So, different percentages of shear walls in braced wall lines and different wall design details will be included in future work to further develop a rapid visual screening tool that supports different levels of design and ages of construction across the existing building inventory.

Lateral force resistance from gypsum wallboard partition walls was not included but will be taken into account in the next phase of the study. Horizontal elements consist of the roof and ceiling. Seismic masses are lumped at the roof level with a uniform distribution over the roof area, including roof, ceiling, partition wall, and shear wall weight. Roof and ceiling dead loads are assumed to be 478 N/m^2 (10 psf) and 191 N/m^2 (4 psf), respectively. Wall dead loads are transferred to the roof diaphragm based on tributary height. Magnitudes of shear wall and partition wall dead loads are based on ASCE 7-05 (ASCE 2005) with a dead load of 527 N/m^2 (11 psf) for exterior shear walls and a uniformly distributed load per floor area of 718 N/m^2 (15 psf) for partition walls.

Structural modeling and analysis was performed using SAPWood v1.0 which incorporates the pancake model (Folz and Filiatrault 2002), the Evolutionary Parameter Hysteretic Model (EPHM) (Pei 2007), and a feature to perform multicase incremental dynamic analysis. In general, the pancake model degenerates an actual 3-dimensional building into a 2-dimensional planar model. Diaphragms (floors and roof) are connected by zero-height shear wall spring elements (Fig. 3). All diaphragms are assumed rigid with infinite in-plane stiffness, so the dynamic responses of buildings can be defined by only 3 degrees of freedom per floor. With this assumption, the model will only be able to capture the effect of torsional moment attributable eccentricity but not the stress concentration at reentrant corners.

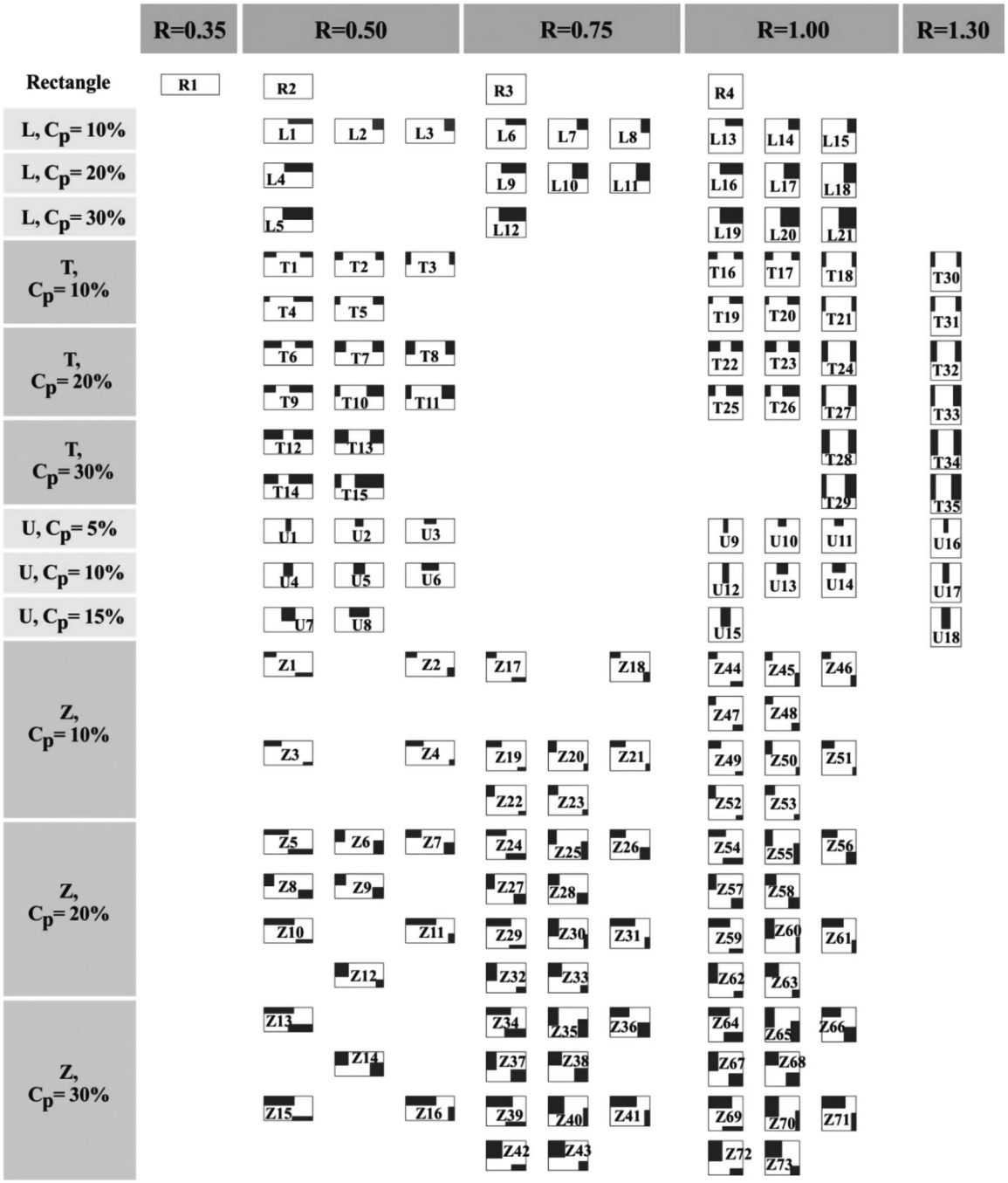

Fig. 2. Summary of configurations based on observations of existing buildings

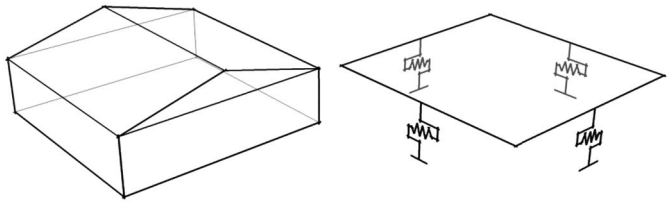

Fig. 3. Rectangular wood-frame house and its pancake model

An EPHM (Pang et al. 2007) was selected to represent the nonlinear force-deformation relationship of shear walls. The model uses exponential functions to trace the descending backbone and hysteresis loop. Incorporated degradation rules for hysteretic parameters allow it to track stiffness and strength degradation. Given appropriate parameters, the EPHM model provides a better simulation of the postpeak envelope behavior than a linearly decaying backbone model, and greater flexibility to represent the actual shear wall hysteresis behavior.

Values of EPHM parameters are from a SAPWood database, generated at the connector level using the SAPWood-NP program, where nail hysteresis data, obtained from cyclic loading tests of nailed sheathing to stud connections (Pei 2007), were used to determine average shear wall parameters. Within the database, parameters for standard shear wall lengths (e.g., 2 ft, 4 ft, and 8 ft) were calculated based on nail connection behavior. Linear interpolation was used to obtain parameters for different wall lengths. Since shear wall configurations of the screened buildings can be different,

it is considered conservative and appropriate to use minimum values in the database for other ductility-related parameters. Nail spacings for edge and field are 15 mm (6 in.) and 30 mm (12 in.), respectively, with a stud spacing of 406 mm (16 in.). EPHM parameters for this specific wall configuration are described in the SAPWood software and user's manual (Pei and van de Lindt 2007).

Dynamic energy dissipation behavior in wood-frame buildings results from both viscous and hysteretic damping. Wood-frame buildings subjected to strong motion are estimated to have an average damping ratio of 10%–20% (Camelo et al. 2001; Folz and Filiatrault 2002), with more damping for larger displacements. For this study, the majority of the damping will be accounted for by nonlinear hysteresis damping in the EPHM springs. A viscous damping ratio of 0.01 was used based on SAPWood model verification (Pei and van de Lindt 2009; van de Lindt et al. 2010), where analyses with a very small viscous damping ratio (usually 0.01) yielded good agreement with shake table test results.

Ground Motions and Structural Analysis

All 151 models were analyzed to determine the maximum lateral drifts in any of the walls. 10 pairs of ground motion time histories developed for Seattle (Somerville et al. 1997), having probabilities of exceedance of 2% in 50 years (typically associated with collapse prevention performance), were used. These ground motions were developed considering 3 types of seismic sources including (1) shallow Seattle crustal faults (at depths less than 10 km), (2) subducting Juan de Fuca plate (at depths of about 60 km), and (3) plate interface at the Cascadia subduction zone (about 100 km west of Seattle). This suite of ground motions includes the 1992 Mendocino, 1992 Erzincan, 1949 Olympia, 1965 Seattle, 1985 Valpariso, 1978 Miyagi-oki, and several simulated ground motions representing deep and shallow interplate earthquakes. Detailed information on these ground motions and their reference numbers which are specified as SE21 to SE40, can be found on the website ⟨http://nisee.berkeley.edu/data/strong_motion/sacsteel/motions/se2in50yr.html⟩.

From Baker (2007), it was observed that "if the records were selected to account for the peaked spectral shape of 'rare' ground motions, then the records could be safely scaled up to represent rare (i.e., high S_a) ground motions while still producing the same structural response values as unscaled ground motions." The selected suite involves rare ground motions, and response spectra for these ground motions (5% damping) are shown in Fig. 4. A similar suite of ground motions was applied to a wide variety of building types and natural frequencies in FEMA (2008), and the selected suite is used for the short period, single-story houses in this study.

The scaling used is unbiased and implemented with the intention to fix the intensity in one excitation direction while keeping the intensity ratio between the two components from the original record, partially because building damage is often driven by excitation in one direction. However, although a common procedure in many situations including shake table testing, this scaling is not as robust as some other possible methods (such as using the geometric means of the two horizontal components).

Each of these ground motions was scaled based on the spectral acceleration (S_a) of a single degree of freedom system with a damping ratio of 0.05 and a natural period of 0.2 s before being applied to the structural models. Twenty S_a targets were used in the study ranging from 0.1 g to 2.0 g at 0.1 g steps. Ground motion scaling was performed so that when the first component of ground motion reached the specified S_a, the same scaling factor was used for the second component. Each orthogonal pair of ground motions was applied twice (rotated 90°) on each model.

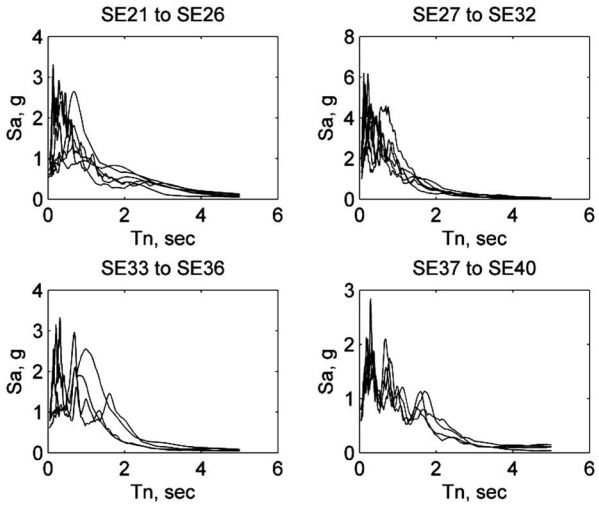

Fig. 4. Response spectra of ground motion records (5% damping)

A total of 60,400 analyses were conducted with 151 models, 10 ground motions each applied twice, and ground motions scaled to 20 different levels. Two different measures of seismic response were determined for each model at each S_a target: (1) median of maximum drifts of shear walls and (2) number of drifts exceeding the 3% collapse prevention limit. Each scaled ground motion pair was applied to the structure twice, thus resulting in 2 sets of outputs. Maximum wall drift from both applications of the ground motion pair was considered the maximum drift for that ground motion, thus giving 10 maximum drifts from 10 ground motion pair inputs. All 10 maximum drifts were used to determine the median maximum drift. Mean maximum drift was not used here since some impractical large drifts are obtained from the numerical analyses. Total number of times that maximum drifts exceeded 3% for a particular spectral acceleration is called number of drifts exceeding 3%. Although not directly related to the probability of collapse, the number of drifts exceeding 3% quantifies the number of events causing severe damage/collapse using the suite of 10 ground motions selected for this study, and allows one to compare extreme performance for different configurations.

Results and Discussion

The overall box area ($a \times b$), overall shape ratio, and percent cutoff are parameters that affect the dynamic characteristics of buildings as they relate to the overall mass and stiffness along both major axes of a floor plan. In this study, the fundamental periods of vibration for all models were found to range from 0.135 s to 0.219 s. Natural periods of the first 3 modes of vibration for each of the worst-case-scenario models (explained in this section) are displayed on top of each model in Fig. 5. In general, the longest natural period corresponds to one of the lateral displacement modes, usually parallel to the short side of the building. The second mode is often the lateral displacement mode in the perpendicular direction. The third mode is typically the torsional mode. Accordingly, the following results can be observed:

- A square shape ($R = 1.0$) better distributes the external shear walls along both major directions, i.e., providing similar stiffnesses. On the other hand, those with long, thin shapes ($R \neq 1.0$) are stiffer in the long direction but more flexible in the short. The square shapes thus tend to have shorter fundamental periods than the more rectangular shapes. For example,

Nat. Hazards Rev., 2012, 13(1): 24-33

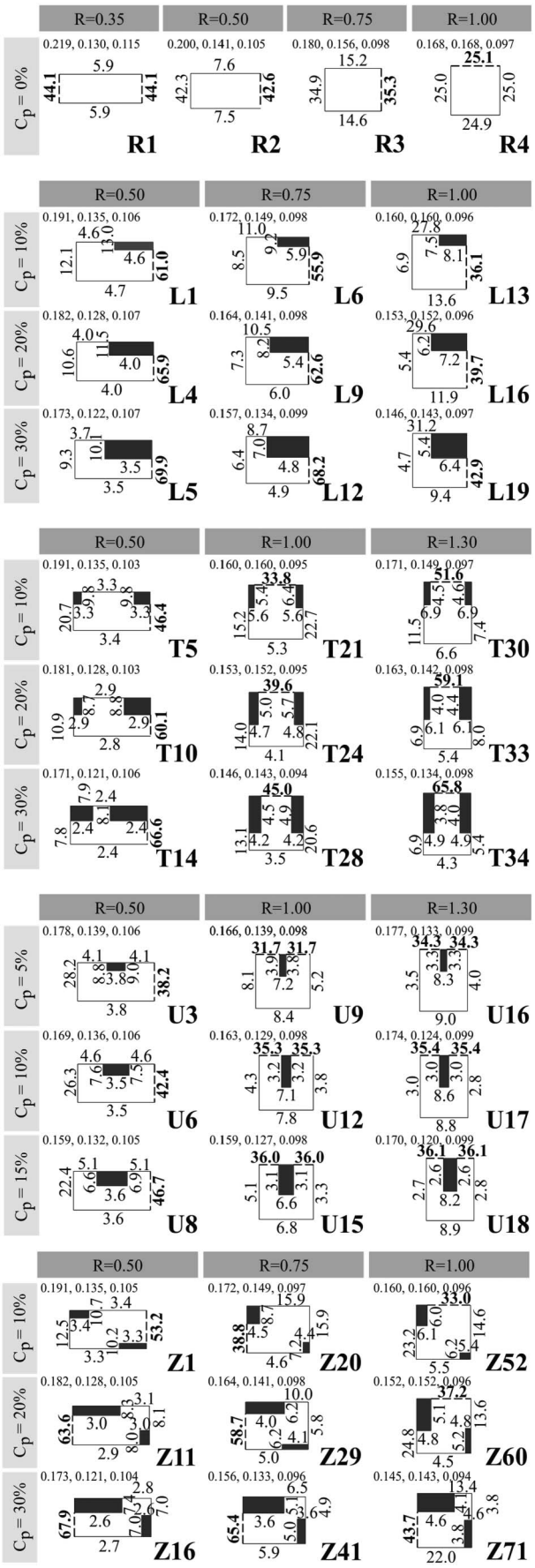

Fig. 5. Summary of selected worst-case-scenario models, percentage of times maximum drifts occur on each wall side, natural periods of first 3 modes of vibration T_1, T_2, T_3 (displayed on top of each model)

the fundamental periods for rectangular shape models (R1, R2, R3, and R4 in Fig. 5) with overall shape ratios of 0.35, 0.50, 0.75, and 1.0 are 0.219 s, 0.200 s, 0.180 s, and 0.168 s, respectively.

- The spacing of the natural periods is also affected by the overall shape of the building. The more slender the plan shape, the larger the spacing between mode 1 and mode 2 periods. Square-like buildings tend to have approximately the same natural periods in modes 1 and 2, except for U-shapes which have increased lateral stiffness in one direction from the walls forming the cutoff area. Natural periods for mode 3 were found to slightly increase as the plan shapes become more slender. For all of these worst-case-scenario models, the average natural periods for the first, second, and third modes are 0.169 s (S.D. = 0.015), 0.139 s (S.D. = 0.012), and 0.100 s (S.D. = 0.005), respectively.
- For plan shapes with a particular combination of overall box area and shape ratio, the larger the percent cutoff area, the shorter the fundamental period. This is because the total seismic mass is reduced whereas the total lateral stiffness in both directions remains the same. For example, for L-shape models (Fig. 5) with $R = 0.5$, the fundamental periods are 0.191 s, 0.182 s, and 0.173 s for 10, 20, and 30% cutoff areas, respectively.

For the same box area, the L, T, U, and Z-shapes have reduced seismic mass compared with the R-shape. Only the U-shape has increased wall mass and increased stiffness. The R-shape thus tends to have the longest fundamental period whereas the U-shape tends to have the shortest. For example, for worst-case-scenario models (Fig. 5) with $R = 0.50$ and $C_p = 10\%$, the fundamental periods for rectangle ($C_p = 0\%$), L, T, U, and Z-shapes are 0.200 s, 0.191 s, 0.191 s, 0.169 s, and 0.191 s, respectively.

The previous results and discussion are for the initial dynamic properties of models. Fig. 6 shows the observed variations in seismic performance when the degradation of shear wall stiffness is included. Fig. 6 is a plot of median maximum drifts versus spectral acceleration for all 151 models. Any median maximum drift that exceeds the 3% collapse prevention limit [73 mm (2.88 in.)] is displayed as 73 mm. This figure shows that, at low S_a (e.g., $S_a \approx 0.0$ g–0.5 g), the variation of median maximum drifts is small with the small ground excitations. The middle range ($S_a \approx 0.5$ g–1.3 g) is where the effect of shape parameters becomes obvious. Median maximum drifts are highly scattered. In this range, U-shapes have the lowest variation partly because of the smaller number of case study samples ($N = 18$). As can be seen from Fig. 2, the total numbers of samples for rectangle, L, T, U, and Z-shapes are 4, 21, 35, 18, and 73, respectively. Another reason is because of the assumption that the cutoff area for the U-shape is center-located (as explained previously). Thus, the eccentricity is developed on one axis only. This is in contrast to Z-shape samples with a larger variation, where the total number of models is 73 and, in addition, changes in the two cutoff areas cause different levels of eccentricity along two major axes. Similarly, large gaps in drifts of the rectangular models are attributable to the nonlinearity and small number of samples ($N = 4$). For the upper range ($S_a > 1.3$ g), most of the median drifts tend to exceed 75 mm, and thus the plots converge to this drift limit.

Effect of Overall Shape Ratio

Figs. 7(a)–7(d) show examples of the correlation between overall shape (aspect) ratio R and median maximum drifts at $S_a = 0.5$ g for L-shapes (percent cutoff $C_p = 30\%$), T-shapes ($C_p = 20\%$), U-shapes ($C_p = 15\%$), and Z-shapes ($C_p = 20\%$), respectively.

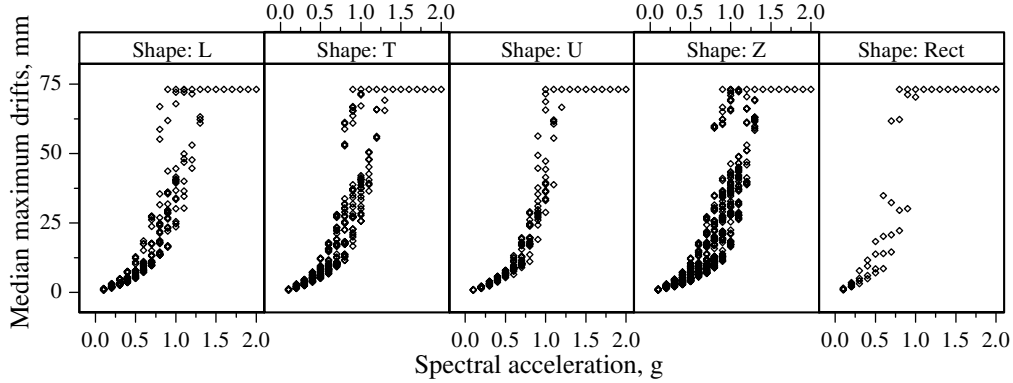

Fig. 6. Median maximum drifts at $S_a = 0.1$ g–2.0 g for all case study models

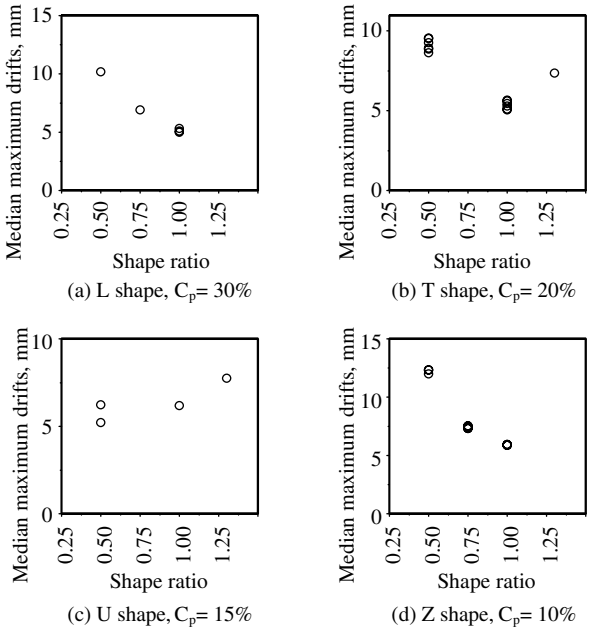

Fig. 7. Effect of shape ratio in terms of median maximum drifts at $S_a = 0.5$ g

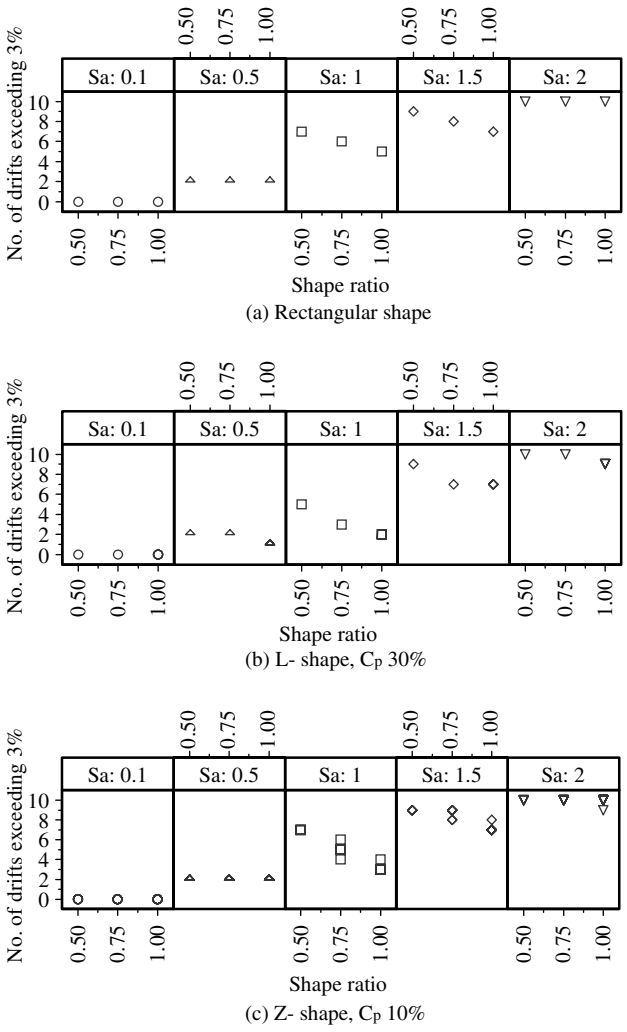

Fig. 8. Effect of shape ratio in terms of number of drifts exceeding 3%

These examples show trends in results over a range of different shapes with different percent cutoffs. For the same total floor area, buildings tend to perform better (smaller drift) as their shape ratios approach 1.0, or as the overall shapes become more square-like. This trend is consistent for all except some U-shapes where performance is observed to be similar or even better at shape ratios less than 1.0. This improvement in lateral load resistance is because extra lengths of shear wall are added on the short side because of the cutoff area in the U-shape. Although this additional wall length enhances the performance for U-shapes with a smaller shape ratio (e.g., $R = 0.5$), it does not appear to benefit larger shape ratios (e.g., $R = 1.0$, 1.3), since lateral load resistance in the other major direction has become more critical.

Fig. 8 shows how overall building shape ratio affects the seismic performance in terms of number of incidences where maximum drifts exceed the 3% collapse prevention limit when excited by the 10 different ground motions. Plots include five levels of S_a: 0.1 g, 0.5 g, 1.0 g, 1.5 g, and 2.0 g. Comparisons are made among buildings with the same shape and total floor area (same percent cutoff). In this comparison, no model exceeded the 3% limit at $S_a = 0.1$ g. For $S_a = 0.5$ g, number of drifts exceeding 3% ranges from 1 to 2 times. At this level, effect of shape ratio is not clearly visible since the spectral acceleration is relatively low. Most ground motions did not cause excessive drifts except for two: the 1992 Mendocino and 1978 Miyagi-oki. Effect of shape ratio (lower number of drifts exceeding 3% as R approaches 1.0) is more obvious for the intermediate range, i.e., $S_a = 1.0$ g and 1.5 g, although most models exceeded the 3% drift limit from all 10 ground motions when $S_a = 2.0$ g.

Nat. Hazards Rev., 2012, 13(1): 24-33

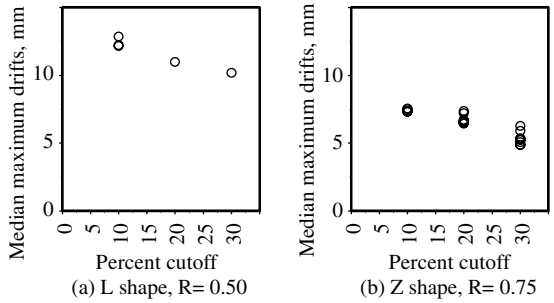

Fig. 9. Effect of percent cutoff in terms of median maximum drifts at $S_a = 0.5$ g

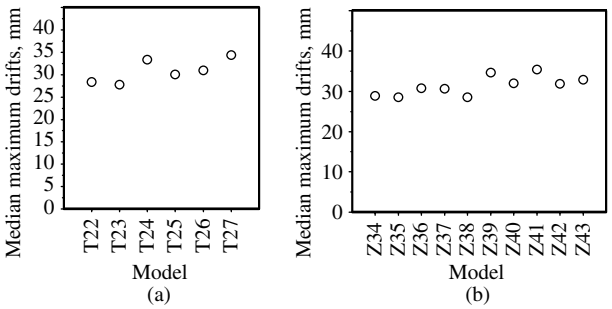

Fig. 10. Effect of cutoff shape ratio and cutoff ratio on median maximum drifts: (a) T-shape, $R = 1.00$, $C_p = 20\%$, $S_a = 1.0$ g; (b) Z-shape, $R = 0.75$, $C_p = 30\%$, $S_a = 1.0$ g

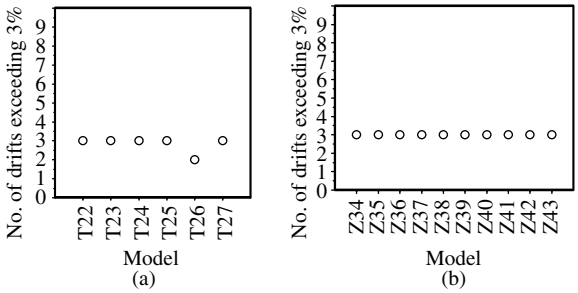

Fig. 11. Effect of cutoff shape ratio and cutoff ratio in terms of number of drifts exceeding 3%: (a) T-shape, $R = 1.00$, $C_p = 20\%$, $S_a = 1.0$ g; (b) Z-shape $R = 0.75$, $C_p = 30\%$, $S_a = 1.0$ g

Effect of Percent Cutoff

For buildings with the same base rectangle ($a \times b$), variation in percent cutoff (from the base rectangle) directly affects at least two factors that influence seismic performance of buildings: eccentricity and seismic mass. By increasing the percent cutoff, the size of reentrant corners increases, and this produces larger eccentricity between centers of rigidity and mass. For example, for L-shape models with $R = 0.5$, the eccentricities along the length and width (e_x, e_y) for L1 ($C_p = 10\%$), L4 ($C_p = 20\%$), and L5 ($C_p = 30\%$) are (0.37 m, 0.05 m), (0.79 m, 0.15 m), and (1.11 m, 0.34 m), respectively. However, increasing the percent cutoff also reduces seismic mass which, in turn, often leads to smaller drift. Results from this study have shown that for buildings with the same base rectangle, maximum drift decreases as percent cutoff increases (Fig. 9). Thus, within the study range, the effect of mass reduction overrides the effect of eccentricity. Examples of this correlation between percent cutoff and median maximum drifts at $S_a = 0.5$ g for L-shapes ($R = 0.50$) and Z-shapes ($R = 0.75$) are shown in Figs. 9(a) and 9(b), respectively.

Effect of Cutoff Shape Ratio

Although cutoff shape ratio (aspect ratio of area cutoff from base rectangle) affects eccentricities along both major axes of a building, within the range studied, it does not cause a major difference in seismic performance for buildings of the same overall shape and total floor area. Fig. 10 shows seismic response in terms of median maximum drifts compared among buildings of the same subindex group (i.e., same shape, overall shape ratio, and percent cutoff), so, differences in drifts result from the variation of cutoff ratio and cutoff shape ratio. Fig. 10(a) shows that, for T-shape models with $R = 1.00$, $C_p = 20\%$, and $S_a = 1.0$ g, median maximum drift varies over a narrow range from 28–34 mm. For Z-shapes with $R = 0.75$, $C_p = 30\%$, $S_a = 1.0$ g [Fig. 10(b)], median maximum drift similarly ranges from 28–35 mm. Comparisons of these two groups are shown again in terms of number of drifts exceeding 3% in Figs. 11(a) and 11(b), where the plots show that, within the range of cutoff area shape ratios and cutoff ratios examined, performances of buildings with the same overall shape, R, and percent cutoff, C_p, are usually identical. Thus, use of one worst-case-scenario model (for example, L1) from each group of sub-sub index buildings (L1, L2, L3) to represent the seismic performance of its corresponding subindex buildings of the same shape, R, and C_p (L-shape, $R = 0.5$, and $Cp = 10\%$) is reasonable.

Selection of a worst-case-scenario model for each subindex level was thus performed by comparison of median maximum drifts over a range of spectral accelerations. The lower bound for comparison is assumed to be the S_a value that induces approximately 12.7 mm (0.5 in.) median maximum drift, whereas the upper bound is that producing 73.1 mm (2.88 in.) median maximum drift (3%). The comparison generally covers approximately a 0.5 g range. The model that has the largest median maximum drift (over the range of spectral accelerations) is considered the worst-case-scenario model for that particular subindex group. Fig. 5 shows a summary of worst-case-scenario models. Comparison of seismic responses in terms of number of drifts exceeding the 3% limit for the selected worst-case-scenario models at $S_a = 1.0$ g is shown in Table 4. In general, the number of simulations with drifts exceeding 3% ranges from 2 to 7, showing building performance differences with changes in plan configuration.

In addition, an unsymmetrical plan tends to cause maximum drift to occur on a particular wall side more often than the others. Generally, the wall located farthest away from the center of rigidity tends to have the maximum drift most frequently. For each worst-case-scenario model, the percentage of times a wall side has either the maximum drift or exceeds 3% drift, resulting from all 400 analyses (10 ground motions pairs applied in 2 orthogonal directions, and 20 spectral acceleration scalings) is summarized in Fig. 5.

Conclusions

Effect of plan configuration on seismic performance of single-story wood-frame dwellings has been examined by (1) establishing a practical configuration range for small, wood-frame dwellings, and proposing an appropriate set of shape parameters, and (2) utilizing a recently developed and verified numerical model for wood-frame building and shear walls for the analyses.

Table 4. Comparison of Seismic Responses in Terms of Number of Drifts Exceeding the 3% Limit Based on the Selected Worst-Case-Scenario Models at $S_a = 1.0$ g

Shape ratio	C_p (%)	Rect.	L	T	U	Z
0.35	0	7	N/A	N/A	N/A	N/A
0.5	0	7	N/A	N/A	N/A	N/A
	5	N/A	N/A	N/A	6	N/A
	10	N/A	7	7	5	7
	15	N/A	N/A	N/A	4	N/A
	20	N/A	7	7	N/A	7
	30	N/A	5	5	N/A	5
0.75	0	6	N/A	N/A	N/A	N/A
	5	N/A	N/A	N/A	N/A	N/A
	10	N/A	6	N/A	N/A	6
	15	N/A	N/A	N/A	N/A	N/A
	20	N/A	3	N/A	N/A	3
	30	N/A	3	N/A	N/A	3
1.0	0	5	N/A	N/A	N/A	N/A
	5	N/A	N/A	N/A	3	N/A
	10	N/A	3	3	3	3
	15	N/A	N/A	N/A	3	N/A
	20	N/A	3	3	N/A	3
	30	N/A	2	2	N/A	2
1.3	5	N/A	N/A	N/A	6	N/A
	10	N/A	N/A	6	5	N/A
	15	N/A	N/A	N/A	5	N/A
	20	N/A	N/A	3	N/A	N/A
	30	N/A	N/A	2	N/A	N/A

Note: N/A = not analyzed configurations.

Seismic performance of small, wood-frame dwellings has been shown (for example, in Table 4) to strongly depend on the overall plan proportions (shape ratio, R) and amount of reduction in area from the base rectangle (percent cutoff, C_p). For buildings with the same floor area, those with square-like base rectangles perform relatively better than those with long, thin base rectangles. For a particular size base rectangle ($a \times b$), maximum shear wall drifts generally decrease as the percent cutoff area (C_p) increases because of reduced mass. Variation of the proportions in cutoff area (cutoff shape ratio R_c), considered within a practical range, has a relatively smaller effect on seismic performance than R and C_p. U-shape buildings with small shape ratio (e.g., $R = 0.5$) can benefit from extra wall length (i.e., increased total stiffness) in the short direction. Such benefits do not occur for U-shapes with shape ratio closer to 1.0 since the critical load resistance direction has changed.

This study reveals the importance of plan configuration identification in efforts such as rapid visual screening. Classification of single-story wood-frame dwellings by shape, size ($a * b$), shape ratio (R), and percent cutoff (C_p) has been shown to be capable of organizing a large population of buildings into a definite number of building groups with similar seismic performance. Plan configuration screening of existing buildings can thus be made by assuming them to perform similarly to the analyzed worst-case scenario models of the same shape, size, R, and C_p.

This approach will be used as a basis for the development of an improved rapid visual screening method considering the complexity of different combinations of configuration, base-rectangular area, numbers of stories, windows, and doors openings, and garage doors. Comparison of results between this approach and the simpler, current FEMA 154 (which simply increases the input spectral acceleration by 50% for a plan irregularity) will be made.

Acknowledgments

The authors are grateful for the financial support of this project by the Royal Thai Government, the School of Civil and Construction Engineering, and the Department of Wood Science and Engineering, Oregon State University.

References

Applied Technology Council. (2007). "Seismic rehabilitation guidelines for detached, single family, wood-frame dwellings." *ATC 50-1*, Redwood City, CA.

ASCE. (2005). "Minimum design loads for buildings and other structures." *ASCE/SEI 7-05*, Reston, VA.

Baker, J. W. (2007). "Measuring bias in structural response caused by ground motion scaling." *Proc., 8th Pacific Conf. on Earthquake Engineering*, Nangyang Technological Univ., Singapore.

Camelo, V. S., Beck, J. L., and Hall, J. F. (2001). "Dynamic characteristics of woodframe structures." *CUREE Publication No. W-11*, Richmond, CA.

Council of American Building Officials (CABO). (1989). "CABO one and two family dwelling code." *CABO 1989 edition*, Falls Church, VA.

Council of American Building Officials (CABO). (1995). "CABO one and two family dwelling code." *CABO 1995 edition*, Falls Church, VA.

Federal Emergency Management Agency (FEMA). (2002a). "Rapid visual screening of buildings for potential seismic hazards: A handbook." *FEMA 154*, Washington, DC.

Federal Emergency Management Agency (FEMA). (2002b). "Rapid visual screening of buildings for potential seismic hazards: Supporting documentation." *FEMA 155*, Washington, DC.

Federal Emergency Management Agency (FEMA). (2008). "Quantification of building seismic performance factors." *FEMA P695*, Washington, DC.

Folz, B., and Filiatrault, A. (2002). "A computer program for seismic analysis of woodframe structure." *CUREE Publication No. W-21*, Richmond, CA.

International Code Council (ICC). (2000). "International residential code for one- and two-family dwellings." *IRC 2000*, Falls Church, VA.

Pang, W. C., Rosowsky, D. V., Pei, S., and van de Lindt, J. W. (2007). "Evolutionary parameter hysteretic model for wood shear walls." *J. Struct. Eng.*, 133(8), 1118–1129.

Pei, S. (2007). "Loss analysis and loss based seismic design for woodframe structures." Ph.D. thesis, Dept. of Civil and Environmental Engineering, Colorado State Univ., Fort Collins, CO.

Pei, S., and van de Lindt, J. W. (2007). "User's manual for SAPWood for Windows." ⟨http://www.engr.colostate.edu/NEESWood/sapwood.shtml⟩ (Dec. 10, 2007).

Pei, S., and van de Lindt, J. W. (2009). "Coupled shear-bending formulation for seismic analysis of stacked wood shear wall systems." *Earthquake Eng. Struct. Dyn.*, 38(14), 1631–1647.

Schierle, G. G. (2003). "Northridge earthquake field investigations: Statistical analysis of woodframe damage." *CUREE Publication No. W-09*, Richmond, CA.

Somerville, P., Smith, N., Punyamurthula, S., and Sun, J. (1997). "Development of ground motion time histories for phase 2 of the FEMA/SAC steel project." *Rep. No. SAC/BD-97/04*, SAC Joint Venture for the Federal Emergency Management Agency, Washington, DC.

U.S. Census Bureau, Population Division. (2009). "Population estimates-vintage 2007 archive." ⟨http://www.census.gov/popest/archives/2000s/vintage_2007/⟩ (Mar. 2, 2009).

van de Lindt, J. W., Pei, S., Liu, H., and Filiatrault, A. (2010). "Three-dimensional seismic response of a full-scale light-frame wood building: Numerical study." *J. Struct. Eng.*, 136(1), 56–65.